Mon. Not. R. Astron. Soc. **296,** 296–305 (1998)

# The EC 14026 stars – V. The pulsation periods of PB 8783

D. O'Donoghue,[1] C. Koen,[2] J.-E. Solheim,[3] M. A. Barstow,[4] P. D. Dobbie,[4] M. S. O'Brien,[5] J. C. Clemens,[6] D. J. Sullivan[7] and S. D. Kawaler[5]

[1]*Department of Astronomy, University of Cape Town, Rondebosch 7700, South Africa*
[2]*South African Astronomical Observatory, PO Box 9, Observatory 7935, Cape, South Africa*
[3]*Institutt for Matematiske Realfag, Universitet i Trømso, 9000 Trømso, Norway*
[4]*Department of Physics and Astronomy, University of Leicester, Leicester LE1 7RH*
[5]*Department of Physics and Astronomy, Iowa State University, Ames, IA 50011, USA*
[6]*California Institute of Technology, Pasadena, CA 91125, USA*
[7]*Department of Physics, Victoria University, Box 600, Wellington, New Zealand*

Accepted 1998 January 5. Received 1997 October 7; in original form 1997 April 7

**ABSTRACT**

PB 8783 is a member of the newly discovered class of pulsating sdB stars, the EC 14026 stars. The potential of the pulsations of these stars as diagnostic probes of their interiors can only be realized fully by intensive campaigns of multisite time series photometry. To this end we have undertaken a campaign spanning 2 weeks and involving data from five different sites. 183 h of data were obtained. Frequency analysis yielded at least 11 pulsation periods in seven discrete groups between 94 and 136 s. Three of the periods in one specific group are equally spaced in frequency, with a spacing of 0.94 μHz. The frequency spacings amongst the members of other groups are similar to this. A rotation period of ~12 d is implied. A general scheme for identifying the observed modes is suggested. The periods from a detailed model are in good overall agreement with the observed periods, but some difficulties remain. Three additional periods in the range 61–63 s, and with very low amplitude, were also found. No convincing interpretation of these could be devised.

**Key words:** binaries: close – stars: individual: PB 8783 – stars: oscillations.

## 1 INTRODUCTION

A new class of pulsating star, the EC 14026 stars, has recently been discovered (Kilkenny et al. 1996, hereafter Paper I). The prototype, EC 14026 – 2647, displays 144-s oscillations with an amplitude of ~1 per cent. Analysis of its spectrum and *UBV* colours suggests that the star is composite, comprising a hot sdB star and an early G, main-sequence companion (O'Donoghue et al. 1996, hereafter Paper IV). The search for other stars of this kind has yielded nine pulsators to date, of which three have been published: EC 10228 – 0905 (Stobie et al. 1996, hereafter Paper III), EC 20117 – 4014 (Paper IV) and, the subject of this paper, PB 8783 (Koen et al. 1996, hereafter Paper II). These three objects also exhibit low-amplitude, short-period pulsations. Atmospheric analyis shows them to have a similar structure to EC 14026 – 2647: an sdB star with a cool main-sequence companion of spectral type F–G (Paper IV). Pulsation modelling (Paper III) indicates that the period of low-order, low-degree radial and non-radial p-modes are consistent with the observed periods.

As discussed in detail in Paper IV, the pulsations are potentially valuable diagnostics of the structure of the sdB star and the binary in which it resides. This potential can only be realized, however, by intensive photometric monitoring. We therefore undertook a campaign to monitor PB 8783 from five sites over a 2-week interval. This particular star was chosen because its pulsations are relatively prominent (fig. 1 of Paper II); in addition, the analysis in Paper II yielded six frequencies, with a promise of more. This paper reports the results of this effort.

## 2 OBSERVATIONS

### 2.1 Equipment

High-speed photometry of EC 20117 – 4014 was obtained using the 1-m telescopes at Mt John University Observa-

tory (MJUO), the South African Astronomical Observatory (SAAO), Cerro Tololo Inter-American Observatory (CTIO) and La Palma (LP). The 2.1-m telescope at McDonald Observatory (McD) was also used. At a declination of $-5°$, PB 8783 is suitably placed for observation from observatories in both hemispheres. At McDonald and La Palma, three-channel photometers were used, providing a record of the programme star, a nearby field star and the sky (Kleinman, Nather & Phillips 1996). In the south, a two-channel photometer was available at Mt John. At CTIO and SAAO, single-channel photometers were used. The intrinsic variations of PB 8783 are oscillations of sufficiently low amplitude that any cloud was immediately evident in the light curve. For the dual- and single-channel photometers, the time series of PB 8783 was interrupted at suitable intervals to obtain measurements of the sky background.

All photometers were equipped with blue-sensitive photomultiplier tubes and were used without a filter. The responses of the systems thus had an effective wavelength similar to Johnson *B*, but with a much broader bandpass. The extent of the red response of these detectors is of some relevance, as the F0 companion to the sdB pulsator in PB 8783 contributes more light at wavelengths longer than ~4000 Å (fig. 7 of Paper II). The amount of (presumably) non-variable 'background' contributed to the measurements by the cool companion may be different, depending on the shape and red cut-off of the responses of the photomultiplier tubes on each photometer. Some consideration was thus given in the subsequent analysis as to whether there were any systematic changes in pulsation amplitude from site to site. All observations were obtained with a time resoluton of 10 s. Altogether 183.5 h of useful observations were obtained, spanning 14.3 d with a duty cycle of 53 per cent. These statistics are best appreciated from inspection of Fig. 1, which shows a plot of all the data; each panel spans 1 d. An observing log is given in Table 1.

### 2.2 Data reduction

The data were reduced on a run-by-run basis with standard techniques: for the three-channel photometer data, the smoothed sky channel was subtracted from the star channel on a point-by-point basis; for the other data, the sporadic sky measurements were interpolated using a cubic spline and subtracted from the programme star measurements. Most of the raw light curves of PB 8783 had an umbrella-shaped appearance, due to the run starting and ending at high airmass, with meridian passage occurring roughly in the middle. It was therefore a straightforward task to determine the mean atmospheric extinction coeficient required to 'flatten' the umbrella shape, thereby correcting for atmospheric extinction. This coefficient varied between ~0.25

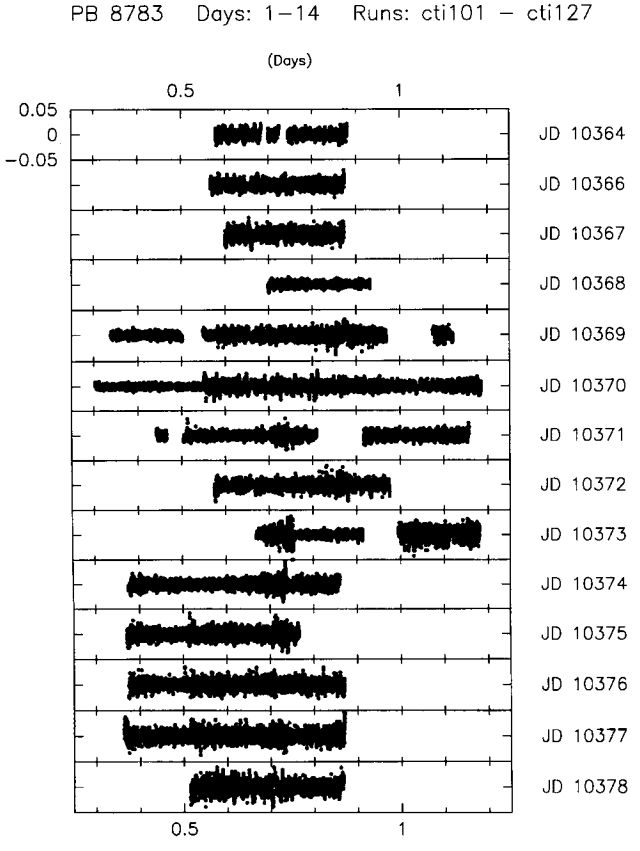


**Figure 1.** Plot of all the data listed in Table 1. Each panel spans 1 d. The corresponding Julian Date (after 244 0000.0) is indicated at the right. The abscissa is labelled with the fractional Julian Date. The ordinate of each panel extends ±5 per cent about the mean brightness of the star.

**Table 1.** High-speed photometry of PB 8783.

| Run Name | Date | Time (UT) | Start of Run BJDD (2450000+) | Length (hr) | Observatory |
|---|---|---|---|---|---|
| cti101 | 08/10/96 | 01:44:00 | 364.57855 | 7.3 | CTIO |
| cti106 | 10/10/96 | 01:28:00 | 366.56744 | 7.6 | CTIO |
| cti108 | 11/10/96 | 02:15:00 | 367.60008 | 6.7 | CTIO |
| jcc-0259 | 12/10/96 | 04:36:00 | 368.69799 | 5.6 | McD |
| S0001 | 12/10/96 | 19:58:00 | 369.33826 | 2.9 | SAAO |
| S0001A | 12/10/96 | 22:53:50 | 369.46037 | 3.7 | SAAO |
| cti114 | 13/10/96 | 01:45:00 | 369.57923 | 7.1 | CTIO |
| jcc-0261 | 13/10/96 | 04:36:00 | 369.69798 | 0.7 | McD |
| jcc-0261 | 13/10/96 | 04:36:00 | 369.69798 | 5.1 | McD |
| oc1396q1 | 13/10/96 | 08:56:00 | 369.87854 | 1.6 | MJUO |
| oc1396q3 | 13/10/96 | 13:41:00 | 370.07645 | 1.1 | MJUO |
| S0002 | 13/10/96 | 19:07:00 | 370.30284 | 7.4 | SAAO |
| cti116 | 14/10/96 | 01:03:00 | 370.55006 | 7.7 | CTIO |
| jcc-0262 | 14/10/96 | 03:50:00 | 370.66603 | 7.3 | McD |
| oc1496q1 | 14/10/96 | 08:27:00 | 370.85839 | 7.9 | MJUO |
| mpj001 | 14/10/96 | 22:27:26 | 371.44202 | 0.6 | LP |
| mpj002 | 14/10/96 | 23:58:00 | 371.50491 | 4.9 | LP |
| mso-0041 | 15/10/96 | 03:57:00 | 371.67088 | 3.3 | McD |
| cti119 | 15/10/96 | 04:47:00 | 371.70561 | 2.3 | CTIO |
| oc1596q1 | 15/10/96 | 09:52:00 | 371.91741 | 5.8 | MJUO |
| cti121 | 16/10/96 | 01:36:00 | 372.57296 | 7.1 | CTIO |
| mso-0042 | 16/10/96 | 06:54:30 | 372.79414 | 3.7 | McD |
| oc1696q1 | 16/10/96 | 08:23:00 | 372.85559 | 2.9 | MJUO |
| mso-0044 | 17/10/96 | 03:55:00 | 373.66947 | 5.8 | McD |
| mpj006 | 17/10/96 | 04:12:00 | 373.68128 | 1.6 | LP |
| oc1796q1 | 17/10/96 | 11:45:00 | 373.99586 | 2.9 | MJUO |
| oc1796q2 | 17/10/96 | 14:44:00 | 374.12016 | 1.5 | MJUO |
| mpj008 | 17/10/96 | 20:52:00 | 374.37571 | 8.5 | LP |
| mso-0045 | 18/10/96 | 03:29:00 | 374.65140 | 3.4 | McD |
| cti123 | 18/10/96 | 04:17:00 | 374.68474 | 4.5 | CTIO |
| mpj009 | 18/10/96 | 20:19:00 | 375.35278 | 8.7 | LP |
| cti124 | 19/10/96 | 00:07:00 | 375.51111 | 6.4 | CTIO |
| mpj010 | 19/10/96 | 20:39:00 | 376.36665 | 8.0 | LP |
| cti125 | 20/10/96 | 00:13:00 | 376.51526 | 8.5 | CTIO |
| mpj011 | 20/10/96 | 20:34:00 | 377.36316 | 8.6 | LP |
| cti126 | 21/10/96 | 00:15:00 | 377.51663 | 8.5 | CTIO |
| cti127 | 22/10/96 | 00:11:00 | 378.51383 | 8.5 | CTIO |

and ~0.35 from site to site. The mean levels of the resulting reduced light curves also varied considerably from site to site, due to differences in telescope aperture, detector sensitivity and state of the primary mirror. Before further analysis was conducted, therefore, all light curves were normalized by their respective mean levels, yielding data in fractional intensity units, d*I*/*I*. Because of the inconvenience of the term 'fractional intensity units', Winget et al. (1994) have named this unit the 'modulation intensity' (mi). One thousandth of an mi will be called 'milli modulation intensity' (mmi), which is related by a scaling factor, 1.0857, to the more conventional mmag unit; the latter is, however, logarithmic in the measured light intensity, whereas the mmi is linear. We shall adopt the mi and mmi throughout this paper, and note by way of example that 10 mmi implies that the star has changed by 1 per cent with respect to its mean brightness.

### 2.3 Light curves and data quality

Fig. 2 shows two light curves obtained at CTIO (run cti119) and McDonald (run mso-0041), plotted on identical vertical and horizontal scales: mso-0041 has been shifted upwards for clarity, whilst cti110 appears as the lower light curve in the panels of Fig. 2. The McDonald data are of excellent quality: beating of two or more periods with a peak-to-peak amplitude of 20 mmi is evident on a time-scale of ~1 h. The peak-to-peak variation in brightness in the data reported in Paper II, 38.5 mmag, is much larger than in the present data (compare Fig. 2 with fig. 1 of Paper II, which is also plotted on the same scale). This is true for all the data acquired during the campaign, a vastly greater data set than that reported in Paper II. The analysis below will show that it is unlikely that these differences are due to beating of closely spaced frequencies. There thus appear to be intrinsic variations in the strength of the oscillations over a long time-scale.

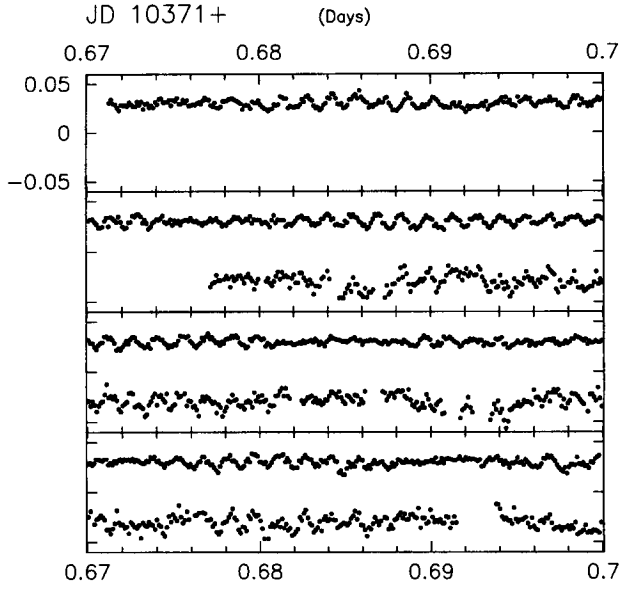


**Figure 2.** Good-quality (upper: mso-0041) and poor-quality (lower: cti119) overlapping light curves of PB 8783. The abscissa is in d, and the ordinate in mi.

A detailed comparison of the McDonald and CTIO data shows that the CTIO data (run cti119) are of much poorer quality. The oscillations can only just be discerned from inspection of the light curve, whereas they are obvious in the McDonald data. Run cti119 is typical of the data obtained at that site; in spite of strenuous efforts to improve the stability of the instrumentation, it was not possible to eliminate the low-frequency variations seen in Fig. 2. Data from the other sites were intermediate in quality between the McDonald and CTIO data. In spite of the modest quality of the CTIO data, the Fourier amplitude spectra derived from these runs were quite acceptable, because the frequency regions of interest were *not* significantly affected by the low-frequency variations visible in Fig. 2.

## 3 TIME SERIES ANALYSIS

### 3.1 The question of low-frequency variations

In Paper II it was noted that low-frequency variations at about 54 and 135 μHz could be present in the light curve, raising the interesting possibility that the cool companion may be a $\delta$ Scuti-type pulsator. In order to check this, the best quality light curves were selected from Table 1 and combined to calculate a Fourier amplitude spectrum (Deeming 1975) between 0 and 1000 μHz. The result yielded a highest peak at 46 μHz and its 1-$d^{-1}$ alias, unrelated to the frequencies proposed in Paper II. In addition, the amplitude of this peak is barely above the residual low-frequency hump of power due to atmospheric transparency variations. We thus find no evidence to support the presence of low-frequency variations in this star.

### 3.2 Surveying the frequency domain

Fourier amplitude spectra between 1000 μHz and the Nyquist frequency of 50 000 μHz were calcuated for all runs. In addition, a Fourier amplitude spectrum of *all* the data, comprising 250 000 frequencies, was also calculated over the same frequency range. No significant peaks were found in any of these spectra in the range 20 000–50 000 μHz. Fig. 3 shows the amplitude spectrum of all the data over the 1000–20 000 μHz range.

Inspection of Fig. 3 shows that the largest peaks lie in the range 7000–9000 μHz. Another peak occurs at ~10 600 μHz. Finally, there is another cluster of peaks in the range 15 000–17 000 μHz. The features and gradual increase in power in the range 1000–2000 μHz arise from residual low-frequency variations due to the atmosphere or instrument, and should be disregarded. Other than the peaks just mentioned, no features attributable to the star with an amplitude exceeding the noise level of 0.1 mmi were found in the range 1000–50 000 μHz.

### 3.3 The 7000–11 000 μHz range

As may be seen in Fig. 3, most of the variability arises from peaks in the 7000–11 000 μHz range. Fig. 4 shows an amplitude spectrum over the 7000–9000 μHz range. It should first be noted that the alias pattern near 8330 μHz arises from the CTIO 1-m telescope drive (an experiment was done to measure the drive period, which was found to be ~120 s).

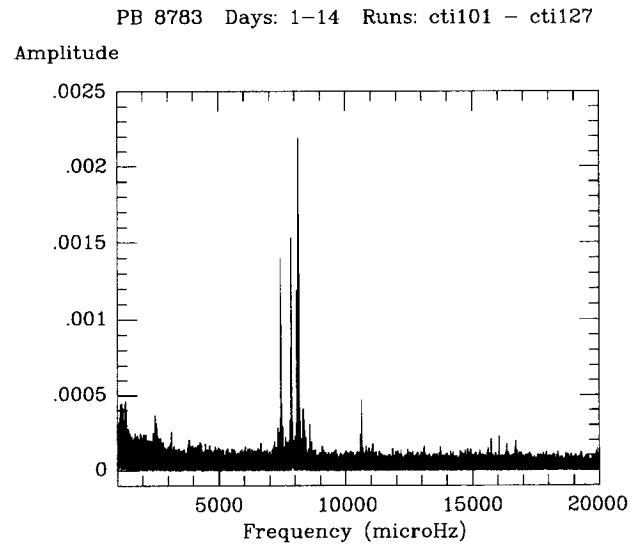


**Figure 3.** Fourier amplitude spectrum of *all* the data in the range 1000–20 000 μHz. The ordinate is in mi.

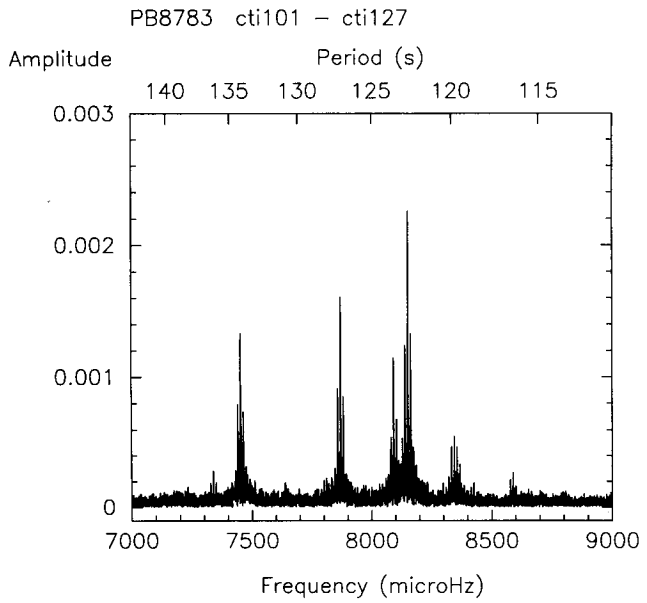


**Figure 4.** Fourier amplitude spectrum of *all* the data in the range 7000–9000 μHz. The ordinate is in mi.

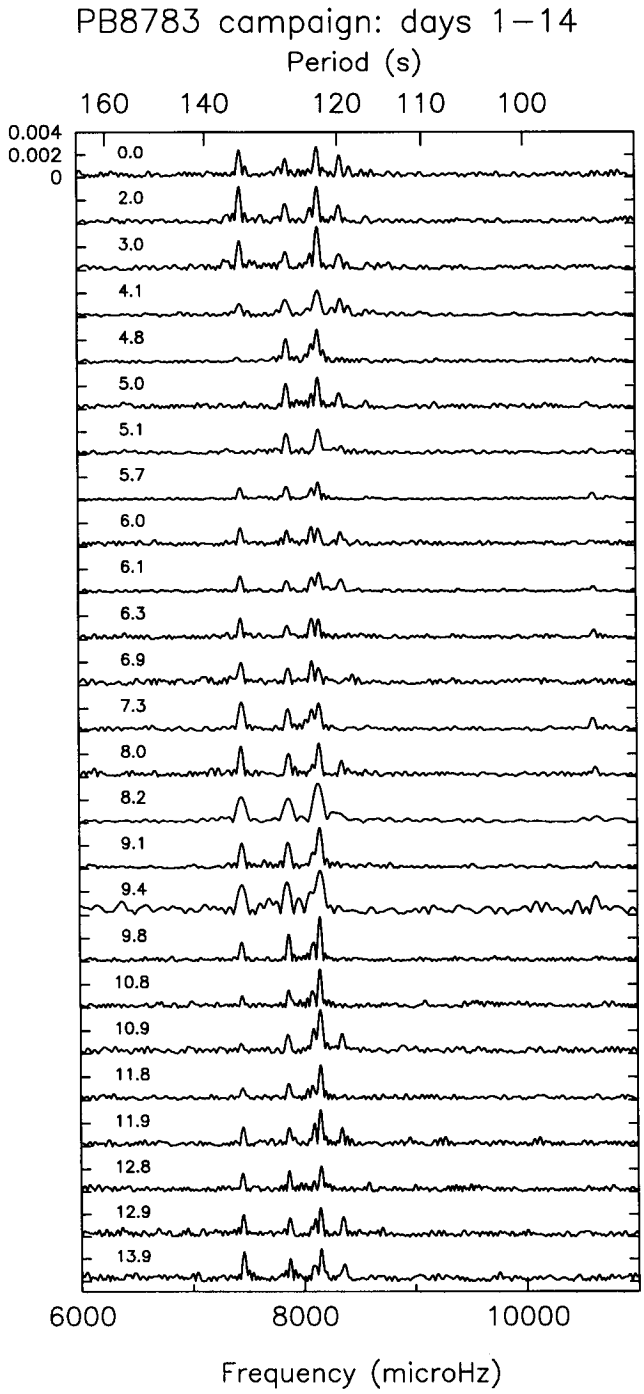


**Figure 5.** Montage of Fourier amplitude spectra of all runs of 4 h in length or longer. The vertical scale is the same for all the spectra. Time increases down the page, and day number relative to the first run is indicated on the left of the panel containing each spectrum.

This signal was found *only* in the CTIO data. It should thus be disregarded.

There are four obvious independent peaks in Fig. 4: at periods of 134.2, 127.1, 123.6 and 122.7 s. In addition, there are smaller but none the less significant peaks at 116.4 and 136.2 s.

In order to explore the behaviour of these peaks, all runs of 4 h or more were selected, and Fourier amplitude spectra were calculated. The results are shown as a montage in Fig. 5. The time of the mid-point of the data subset, in d, relative to that of the first run is shown in the top left-hand corner of each panel;. Each amplitude spectrum is plotted on the same vertical scale. The most noticeable feature of Fig. 5 is the ampitude modulation of the 134-s period, which essentially disappears twice during the campaign. Careful scrutiny reveals that *all* peaks in Fig. 5 vary in amplitude, including the 94-s peak (which is very weak). Clearly, further investigation of this behaviour is desirable; to achieve this, the best values for the 134-, 127- and 122-s periods were derived by a non-linear least-squares fit to the entire data set. The individual runs were then divided into sections, and the corresponding best periods were fitted to

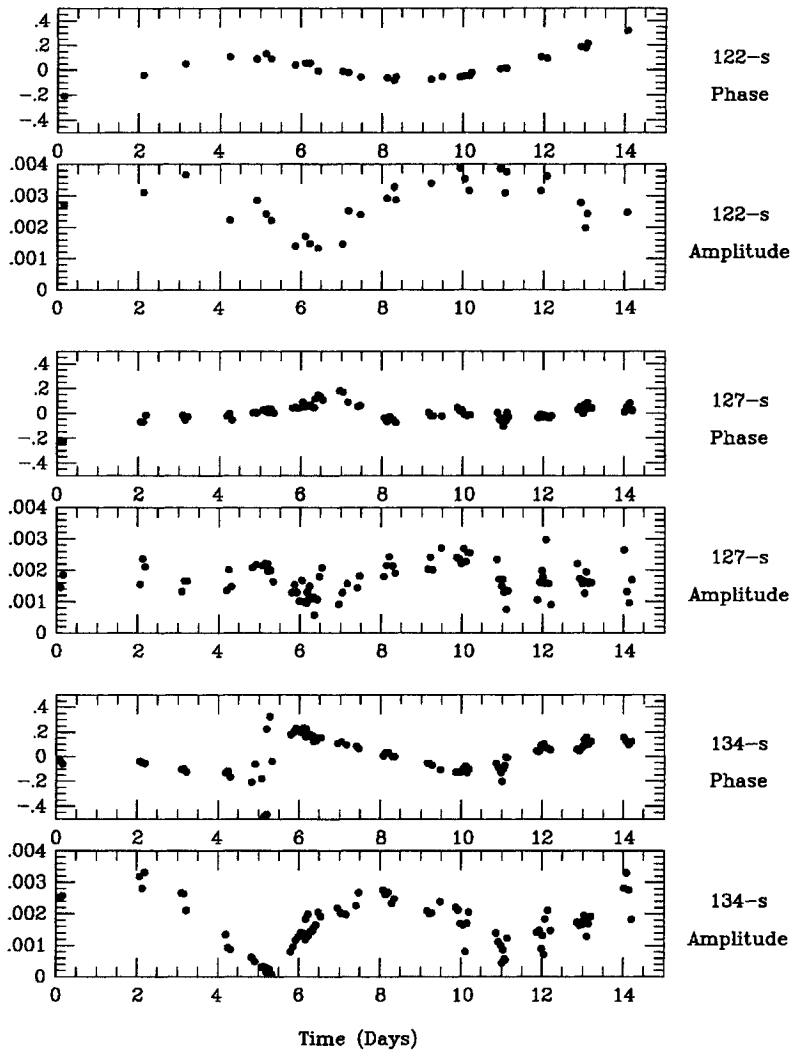


**Figure 6.** Plot of phase and amplitude of the 122-s (top), 127-s (middle) and 134-s (bottom) oscillations versus time. The abscissa of all panels is in d, counted from JD 245 0364.0. The ordinate units of the phase plots are cycles, and of the amplitude plots are mi.

the individual sections by least-squares, yielding an amplitude and a phase relative to the best fit of that period to all the data. For the 134- and 127-s periods, 10 000-s sections were chosen, with 50 per cent overlap (to achieve a slight smoothing of the results). Because of the proximity and therefore possible contamination by the 123-s period, 20 000-s sections were chosen for the 122-s period calculations, also with 50 per cent overlap. The result of these computations is shown in Fig. 6. The 134-s period is modulated in both phase and amplitude with a period of $\sim$6 d. There is clearly some modulaton of both the amplitude and phase of the 127-s period, but it is not clear whether or not it is periodic; from the amplitude plot, there is a suggestion that it may also occur on a time-scale of 6 d, but this claim is not secure. The phase of the 122-s period shows a very smooth modulation, while the amplitude of this signal appears to vary with a longer period than that of the 134-s period, approxiamtely 8 d (but this number is not tightly constrained).

The oscillation amplitudes shown in Figs 5 and 6 were calculated from data from all the sites. We inspected these data for systematic differences depending on the site and could find none greater than the errors of measurement. There is thus no sign that the different instrumentation has affected the amplitudes derived in the time series analysis.

The amplitude and phase variations of the strongest signals in the 7000–9000 μHz range have given an initial impression of the frequency structure of these signals. Now, however, we turn to calculations of Fourier amplitude spectra to reveal the details more clearly. The procedure we shall follow is simple. First, the Fourier amplitude spectrum of all the data will be calculated. Then, assuming there are no aliasing ambiguities, the frequency of the highest peak will be fitted to the data by least-squares and subtracted (a process commonly called 'pre-whitening'). The amplitude spectrum of the residuals is then computed and the process repeated until the data are consistent with noise, or aliasing prevents an unambiguous selection of the correct frequency.

### *3.3.1 The 134-s period*

Fig. 7 shows a sequence of Fourier amplitude spectra in a frequency interval surrounding the 134-s period. The top

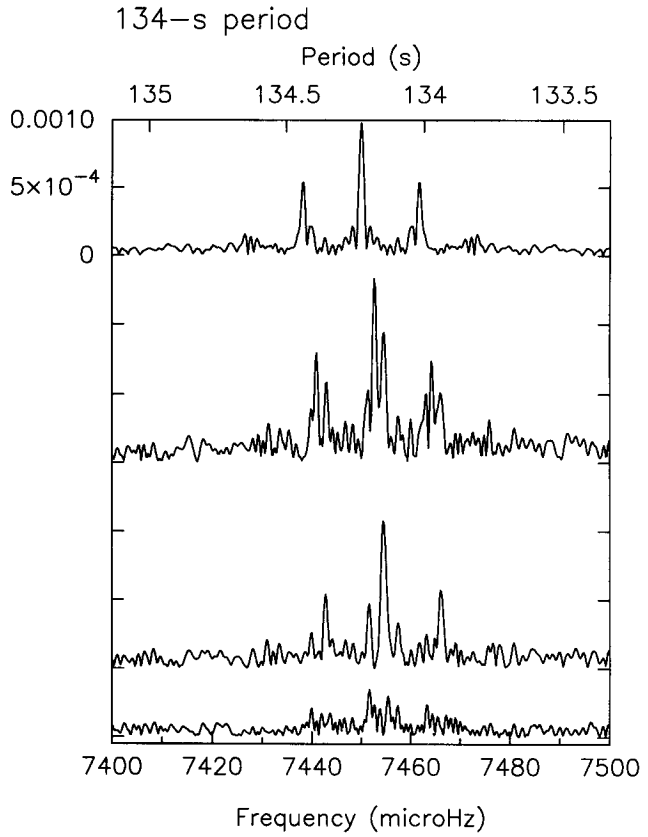


**Figure 7.** The top plot shows the spectral window shifted to 7450 μHz and scaled to 0.001 at zero frequency. The second from the top shows the Fourier amplitude spectrum of all the data for the 134-s period. Successive plots going down the panel are amplitude spectra, calculated by pre-whitening the data with the higheset peak in the previous spectrum. The vertical scale is the same for all the amplitude spectra, and is in units of mi. The zero levels of the amplitude spectra are, respectively, 3, 6 and 7 ordinate carets below that of the spectral window.

spectrum shows the spectral window (Deeming 1975) centred (arbitrarily) on a frequency of a 7450 μHz. Immediately below is the Fourier amplitude spectrum of all the data. A comparison of these two plots shows that there is more than one frequency present in the second plot, and that there is no difficulty with selecting the highest peak as the correct alias. When the data are pre-whitened by this frequency, the third spectrum results. Once again the correct alias can be selected and pre-whitened from the data, leaving the bottom spectrum. There is clearly power in excess of the noise in this last spectrum, but the highest peak may not be the correct choice. Examining the frequency of this peak and plausible alternatives did not reveal any pattern of equal splitting or other grounds for making a choice (as discussed in Section 4, equally split frequency components are a characteristic of non-radial pulsation). We therefore merely draw attention to the fact that additional component(s) are probably present.

We have determined the frequency, amplitude and phase of the two definite signals by a non-linear least-squares fit of these frequencies to the data simultaneously. The results

**Table 2.** Results of the frequency analysis.[1]

| Group Name | Frequency ($\mu$Hz) | Period (s) | Amplitude (mmi) | $T_{max}$ BJDD (2450364+) |
|---|---|---|---|---|
| 136-s | 7338.40 | 136.269 | 0.28 | 0.57819 |
| | 10 | 2 | 5 | 1 |
| 134-s | 7452.52 | 134.183 | 1.78 | 0.57808 |
| | 10 | 1 | 2 | 1 |
| | 7454.42 | 134.146 | 1.09 | 0.57865 |
| | 10 | 1 | 4 | 1 |
| 127-s | 7870.32 | 127.060 | 1.62 | 0.57894 |
| | 10 | 2 | 4 | 2 |
| 123-s | 8092.08 | 123.578 | 1.20 | 0.57912 |
| | 10 | 2 | 5 | 2 |
| 122-s | 8151.63 | 122.675 | 2.09 | 0.57878 |
| | 10 | 2 | 5 | 3 |
| | 8150.68 | 122.689 | 1.65 | 0.57876 |
| | 10 | 2 | 7 | 2 |
| | 8152.56 | 122.661 | 1.18 | 0.57816 |
| | 10 | 2 | 8 | 4 |
| 116-s | 8589.72 | 116.418 | 0.27 | 0.57900 |
| | 10 | 2 | 4 | 1 |
| 94-s | 10587.21 | 94.454 | 0.17 | 0.57906 |
| | 10 | 1 | 4 | 10 |
| | 10623.24 | 94.133 | 0.38 | 0.57819 |
| | 10 | 1 | 4 | 6 |

[1] Uncertainties in the derived quantities are indicated on the next line and are in units of the last significant figure.

are shown in Table 2. With some experimentation, we discovered that the precise values of the two frequencies changed slightly but significantly from the initial values provided by the Fourier transform. Thus these values depend to some extent on the data analysis technique and are not securely determined; we quote conservative errors for these quantities.

The frequency difference between the two components, 1.9 μHz, corresponds to a 'beat' period of 6.1 d and explains the 6.1-d beat period already seen in Fig. 6. The time base of the data set, 14 d, is only just enough to resolve the components seen, which is probably why their values are not precisely determined.

### *3.3.2 The 136-s period*

As can be seen in Fig. 4, there is a small but significant peak with a retinue of aliases at a frequency slightly smaller than 7350 μHz. This peak has nothing to do with the components or aliases of the 134-s period discussed in the last subsection. We calculated an amplitude spectrum (not shown) and, after pre-whitening by the largest (unambiguous) peak, found that the spectrum of the residuals was consistent with noise in this frequency region. We again determined the parameters of this single frequency component by a non-linear least-squares fit; the results are listed in Table 2.

### *3.3.3 The 127-s period*

As in Fig. 7, the top spectrum in Fig. 8 is the spectral window centred on 7870 μHz. The middle plots is the amplitude spectrum of all the data. When the frequency of its highest peak is removed from the data, the lowest spectrum results. It is clear that the lowest spectrum contains at least one, and probably multiple, additional components, but selecting the correct peak is impossible. All that can be said is that it is likely that these additional components are separated from the dominant frequency by a few μHz or less. The parameters of the single, unambiguously determined component are listed in Table 2.

### *3.3.4 The 122-s period*

The top plot in Fig. 9 is the amplitude spectrum of all the data (the spectral window is not repeated in this plot but can be seen in Figs 7 and 8). Once again, there is no problem with aliasing and the highest peak can be selected, pre-whitened from the data, and the spectrum of the residuals computed. This procedure gives rise to the subsequent three spectra in Fig. 9. The parameters of the three strongest peaks in Fig. 9, estimated in the usual way by non-linear least-squares, are listed in Table 2. It is highly significant that, within the errors of measurement, these three peaks are equally split in frequency by $0.94 \pm 0.10$ μHz.

The highest peak in the lowest plot in Fig. 9 is of doubtful significance, and is not included in the components listed in Table 2.

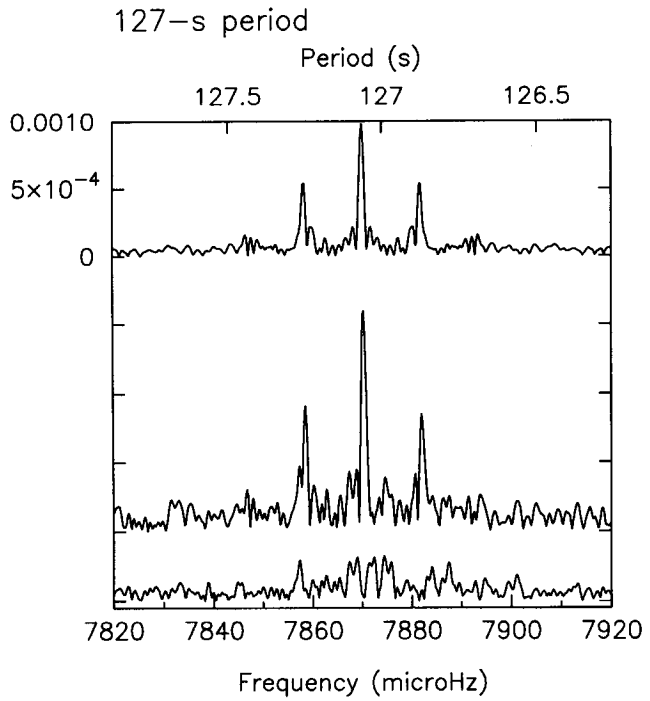


**Figure 8.** As for Fig. 7, except that the amplitude spectra for the 127-s period are shown. The zero levels of the amplitude spectra are, respectively, 4 and 5 ordinate carets below that of the spectral window.

### *3.3.5 The 123-s period*

Inspection of Fig. 4 shows that the alias pattern of the 123-s period is located on the flank of that of the 122-s period. Accordingly, the components of the 122-s period derived in the last subsection were removed from the data, and the resulting amplitude spectrum in the region of the 123-s period appears as the top plot in Fig. 10. The second plot results from pre-whitening the frequency of the highest peak in the top plot. It is clear that there is at least one and possibly more components remaining. As an illustration, we have chosen to extract an additional three components, simply by selecting the highest peak for pre-whitening and calculating the amplitude spectrum of the residuals. The results are shown in the lowest three amplitude spectra in Fig. 10. *We should emphasize that we are far from confident that the number and parameters of these components are reli-*

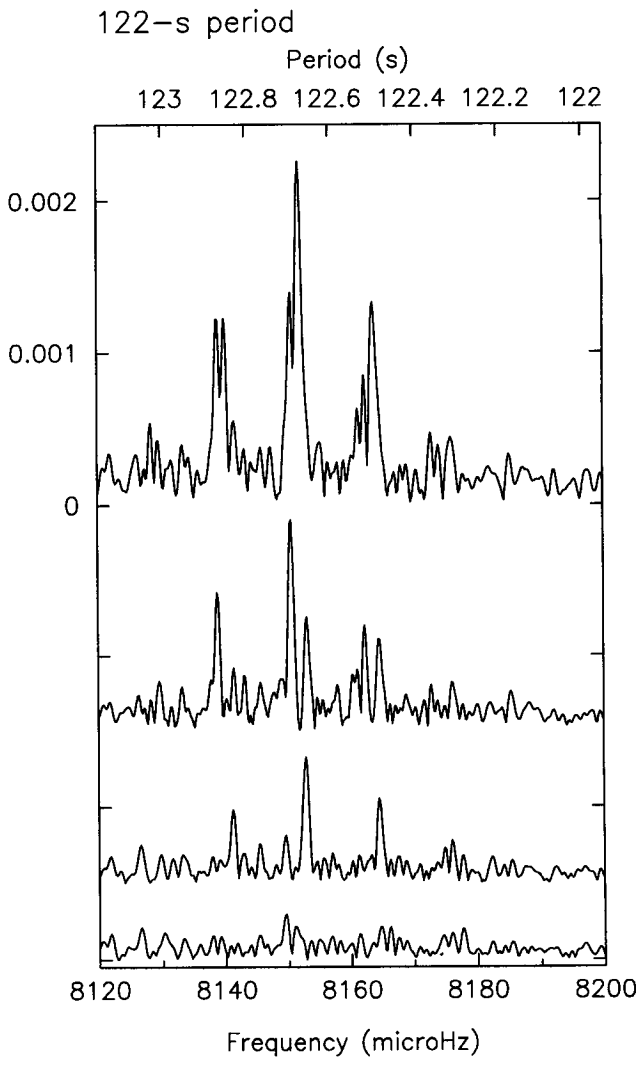


**Figure 9.** The top plot shows the Fourier amplitude spectrum of all the data for the 122-s period. Successive plots going down the panel are amplitude spectra, calculated by pre-whitening the data with the highest peak in the previous spectrum. The vertical scale is the same for all the amplitude spectra, and is in units of mi. The pre-whitened amplitude spectra have been shifted downwards for clarity by arbitrary amounts.

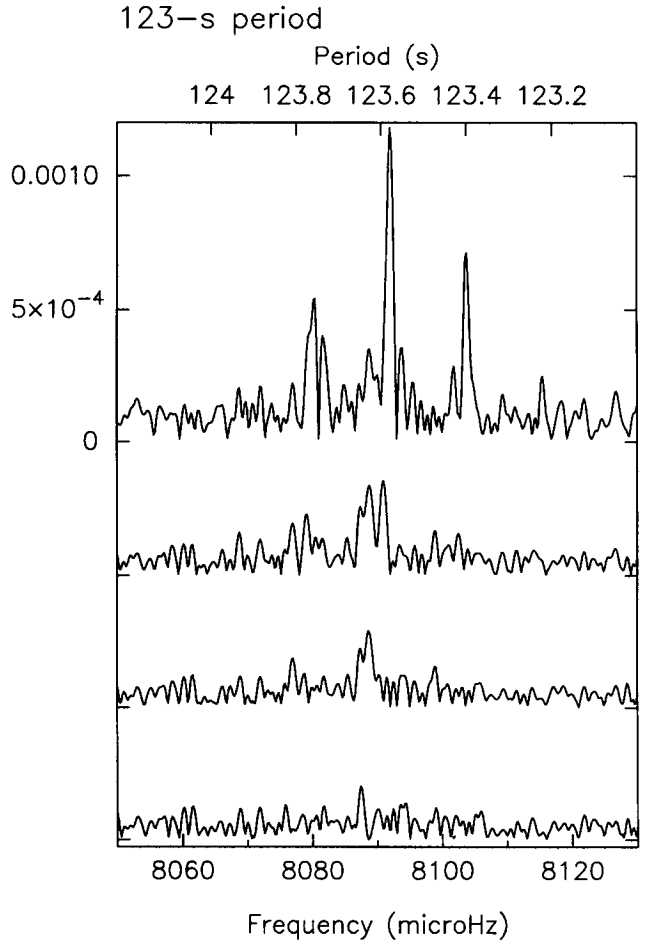


**Figure 10.** As for Fig. 9, except that the Fourier amplitude spectra for the 123-s period are shown. The vertical scale is the same for all the amplitude spectra, and is in units of mi. The pre-whitened amplitude spectra have been shifted downwards by, respectively, 1, 2 and 3 ordinate carets.

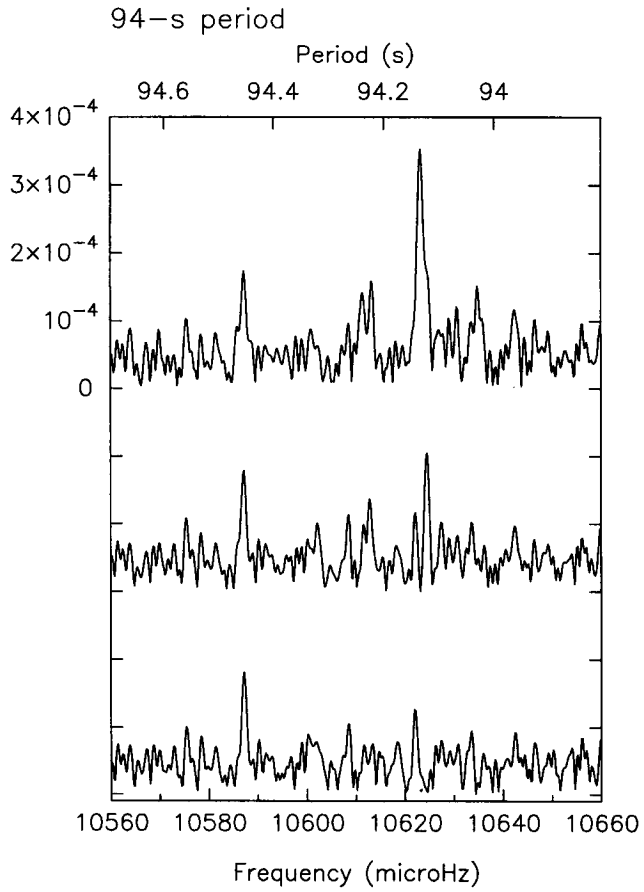


**Figure 11.** As for Fig. 9, except that the Fourier amplitude spectra for the 94-s period are shown. The vertical scale is the same for all the amplitude spectra, and is in units of mi. The pre-whitened amplitude spectra have been shifted downwards by, respectively, 3 and 6 ordinate carets.

*ably determined*. We thus avoid listing the results, and include in Table 2 only the parameters of the one reliably determined frequency.

### *3.3.6 The 116-s period*

Neglecting the power around 120 s (noted already as arising from the CTIO telescope), the last region in Fig. 4 to contain significant power is near 8690 μHz. The principal frequency here is weak. When the data are pre-whitened by this signal, there is a suggestion that additional power may be present at a separation of ~2 μHz. However, any such additional peaks are very weak, and it is more difficult to select the correct peak than in the case of the 123-s components. We therefore list only the principal frequency in Table 2.

### *3.3.7 The 94-s period*

There is clear evidence in Figs 3 and 4 of significant power near 94 s. The top plot in Fig. 11 shows the Fourier amplitude spectrum of all the data in this region. In the usual way, the spectra below were obtained by pre-whitening the data with the frequency of the highest peak in the spectrum immediately above. In addition to the largest amplitude peak in the top plot, the middle plot suggests that there is an additional component at ~10 590 μHz. There *may* also be another component very close (~1.4 μHz) to the largest peak in the top plot, but it is of questionable significance, and we list in Table 2 the parameters of only two components.

## 4 DISCUSSION

In Paper II six frequencies were derived from two short but independent subsets of data. Bearing in mind that the resolution of the amplitude spectra calculated from these two data subsets is considerably worse than in the data reported here, five of the six frequencies (or aliases thereof) listed in Paper II (table 2) are also recovered in the present data as listed in Table 2. Only the 120.62 s period mentioned in Paper II is not found here; as stated already, although a 120-s period was found in the present data, it was only in the CTIO runs whose telescope has a 120-s drive period and is thus believed to be spurious.

From the theory of stellar pulsationi (e.g. Cox 1980), each normal mode of oscillation of a star is associated with three

'quantum' numbers: $n$ (sometimes called $k$), $\ell$ and $m$. The order, $n$, is the quantum number associated with the radial eigenfunction. $\ell$ is associated with the spherical harmonic degree, and gives the number of nodes of the eigenfunction over the surface of the star. Because a large number of nodes leads to geometric cancellation of the oscillations when integrated over the disc of the star, it is generally believed that only small values of $\ell$, say $\ell < 4$, are likely to be detected photometrically. The azimuthal quantum number, $m$, can take on $2\ell+1$ values from $-\ell$ to $+\ell$. In a non-rotating star, the frequencies of these $2\ell+1$ modes are identical. On the other hand, stellar rotation removes the degeneracy of these modes, and their frequencies are then given by the Ledoux (1951) rotational-splitting formula:

$$\nu_{n\ell m} = \nu_{n\ell} + m\Omega(1 - C_{n,\ell}),$$

where $\nu_{n\ell}$ is the pulsation frequency in the non-rotating star, $\Omega$ is the rotation frequency of the star, and $C_{n,\ell}$ is a function of the structure of the star and the mode under consideration. In sdB stars, $C_{n,\ell}$ is typically smaller than $\sim 20$ per cent. Rotational splitting thus results in a set of frequencies which are equally split in frequency by an amount roughly equal to the rotation frequency of the star. Modes with $\ell = 1$ may appear as triplet if all three components are excited to observable amplitudes, $\ell = 2$ modes may appear as quintuplets, etc. It is important to note that $\ell = 0$ (radial) modes should not show rotational splitting under normal circumstances.

With this information, we can now give an overall interpretation of the periods observed in PB 8783 and listed in Table 2. First, note that the observed periods in PB 8783 lie in 'groups', as designated by the Group Name heading in Table 2. These groups comprise one or more individual periods. On the one hand, the frequency spacing between the members of a specific group is small, typically 1–2 μHz. On the other hand, the frequency spacing between the groups is very much larger: at least 60 μHz for the 122- and 123-s periods, which are the closest groups.

In pulsation models of sdB stars, the frequency spacing between modes with different $n$ and/or $\ell$ is occasionally very small (e.g., for $n = 3$, $\ell = 0$, 2 in Table 3). Most spacings, however, are much larger (Table 3, or table 3 of Paper III). These considerations suggest that a specific value of $n$ and $\ell$ can be associated with each observed group. Although the exact values of $n$ and $\ell$ must await detailed modelling, small values are implied. We can then understand the individual periods within the groups as rotationally split multiplets. This claim is supported by the facts that (i) an equally split triplet was seen in the 122-s group, and (ii) the frequency differences between members of the same group do not vary much from group to group, as expected from the Ledoux formula. (Unfortunately, the frequency differences seen within a group are similar to the resolution of the data, $\sim 0.8$ μHz, and are thus not precisely determined.)

Although the presence of only one component in a group (e.g., the 136- or 116-s periods) might suggest the absence of rotational splitting and that the pulsation mode is radial ($\ell = 0$), it should be remembered that these components are near the limit of detection, and that additional components may be present below the detection threshold. The presence of multiple components within a group strongly suggests that for these groups, $\ell$ is non-zero. In the case of the 122-s multiplet, if we assume that the three components seen comprise a triplet with $\ell = 1$, $m = -1$, 0, $+1$, the rotation period of the sdB star in PB 8783 is roughly 12 d.

**Table 3.** Pulsation periods of an evolved EHB sdB star with $T_{\rm eff} = 33\,892$ K, $\log g = 5.770$.

| Degree $\ell$ | Radial Index $n$ | Splitting Coefficient $C_{n\ell}$ | Model Period (s) | PB 8783 Period (s) |
|---|---|---|---|---|
| 2 | 5 | 0.081 | 95.785 | 94.1 |
| 1 | 5 | 0.009 | 101.12 | |
| 3 | 4 | 0.038 | 102.40 | |
| 0 | 4 | – | 104.75 | |
| 2 | 4 | 0.080 | 106.02 | |
| 1 | 4 | 0.014 | 115.73 | 116.4 |
| 3 | 3 | 0.055 | 118.96 | |
| 0 | 3 | – | 122.13 | 122.7 |
| 2 | 3 | 0.071 | 123.10 | 123.6 |
| 3 | 2 | 0.012 | 128.71 | 127.0 |
| 1 | 3 | 0.010 | 129.14 | |
| 0 | 2 | – | 135.04 | 134.2 |
| 2 | 2 | 0.143 | 136.25 | 136.3 |
| 3 | 1 | 0.123 | 142.23 | |

To check the above inferences, we computed models of evolving sdB stars that might be appropriate to PB 8783. These models, constructed using the standard techniques of horizontal branch modelling, were evolved off of the zero-age extended horizontal branch (ZAEHB). This preliminary grid had $Z = 0.02$ and a helium core mass of 0.466 $M_\odot$, with varying hydrogen layer thickness. Some details of how these models and periods were calculated are described in Paper III; the models will be described in more detail in a subsequent paper. We compared the pulsation periods present in the models to those identified in PB 8783. Among the models available, the model with the closest fit to the observed periods turned out to have a total mass of 0.4663 $M_\odot$, and had evolved to a central helium abundance of 0.00613, that is, near the point of core helium exhaustion.

Table 3 shows the pulsation periods for low values of $n$ and $\ell$ for the p-modes of the best-fitting sdB model. This model has an effective temperature and gravity ($T_{\rm eff} = 33\,982$ K, $\log g = 5.770$) which are within the uncertainties of those found in PB 8783 and other EC 14026 stars. We stress that this is a very preliminary identification; the periods in the table above show that models of evolved EHB stars, in general, can reproduce the observed periods. More secure mode identifications, and therefore constraints on the properties of PB 8783, will be possible only after a more exhaustive exploration of the parameters needed to describe stars in this region of the HR diagram. Small changes in the evolutionary state of the model, for example, can change the periods of given modes by more than the difference between the observed mode periods and those of this model. In addition, the observed splitting within the 122-s group indicates that this mode is not an $\ell = 0$ mode, as suggested by the model. Similarly, the 134-s group shows a clear splitting, and therefore cannot be an $\ell = 0$ mode. A comprehensive grid of models is needed before an entirely

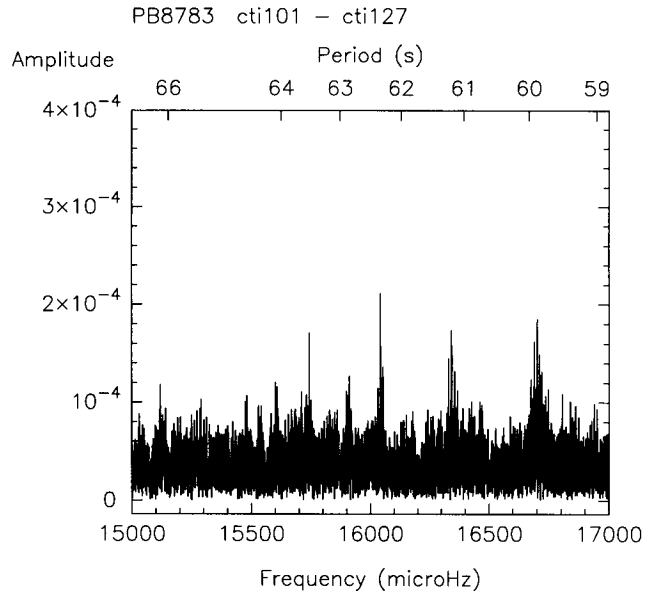


**Figure 12.** Fourier amplitude spectrum of all the data in the range 15 000–17 000 μHz. The ordinate is in mi.

satisfactory fit to the observed periods in PB 8783 can be obtained.

### 4.1 The 15 000–17 000 μHz range

As noted already from Fig. 3, there is evidence for significant power in the 15 000–17 000 μHz range. Fig. 12 shows a Fourier amplitude spectrum of this interval. The cluster of aliases near 16 700 μHz should be disregarded, as it arises from the first harmonic of the 120-s telescope drive period in the CTIO data. Apart from this feature, there are probably three significant peaks in Fig. 12. (Inspection of Fig. 3 shows how these peaks protrude above the general noise level.) They occur at freqauencies of $15\,742.7 \pm 0.1$, $16\,042.7 \pm 0.1$ and $16\,342.1 \pm 0.1$ μHz. The most obvious interpretation of these frequencies is either that they are harmonics of the frequencies listed in Table 2, or that they are 'sum' frequencies of the form $f_i + f_j$, where $f_i$ and $f_j$ are frequencies from Table 2. In either case, this would indicate that the pulsations of PB 8783 have a non-linear character, in spite of their low amplitude. However, all harmonics and 'sum' combinations of the frequencies in Table 2 were tried, but none were found to be consistent with the three frequencies seen in Fig. 12.

Another possibility is that they are simply high order p-modes. Note that the frequency spacings between the three components are $300.0 \pm 0.1$ and $299.4 \pm 0.1$ μHz. Although not precisely equally spaced, the spacings are not far from equal. While equal spacing is what is expected for the asymptotic limit of high order p-modes of the same $\ell$, models of sdB stars at or near the correct effective temperature and gravity have asymptotic spacings of 1500 or 1900 μHz. Therefore it is not likely that these represent high-overtone p-modes of the same $\ell$.

### 4.2 Prospects

Progress in understanding the pulsations of PB 8783 must await secure mode identifications. Although the agreement of the detailed model of Table 3 is encouraging, some problems remain. A comprehensive grid of models covering the vicinity of the $\log g$–$T_{\rm eff}$ plane occupied by PB 8783 is needed to search for a better model and check its uniqueness. It seems likely that further observational assistance in mode identification will be required: the weaker components of the 123- and 127-s oscillations are extremely uncertain (on the basis of the current data), but may provide vital clues in desciphering the rotational splitting. Even the splitting of the 122-s period is not securely measured. An ambitious campaign, aimed at acquiring substantially more than the 183 h of data reported here, will thus have to be arranged.

## ACKNOWLEDGMENTS

MAB and PPD acknowledge the support of the Particle Physics and Astronomy Research Council (PPARC). JES and MAB acknowledge the support of European Union grant CHRXCT 94-034 used to upgrade the La Palma photometer from two to three channels. JES thanks the European Union for travel and subsistance grants while observing. DJS thanks Mt John Observatory for the allocation of telescope time. SDK acknowledges support through the NASA Astrophysics Theory Program and the NSF Young Investigator Programs.

## REFERENCES

Cox J. P., 1980, Theory of Stellar Pulsation. Princeton Univ. Press, Princeton, New Jersey
Deeming T. J., 1975, Ap&SS, 36, 137
Kilkenny D., Koen C., O'Donoghue D., Stobie R. S., 1996, MNRAS, 285, 640 (Paper I)
Kleinman S. J., Nather R. E., Phillips T., 1996, PASP, 108, 356
Koen C., Kilkenny D., O'Donoghue D., van Wyk F., Stobie R. S., 1996, MNRAS, 285, 645 (Paper II)
Ledoux P., 1951, ApJ, 114, 373
O'Donoghue D., Lynas-Gray A. E., Kilkenny D., Stobie R. S., Koen C., 1996, MNRAS, 285, 657 (Paper IV)
Stobie R. S., Kawaler S. D., Kilkenny D., O'Donoghue D., Koen C., 1996, MNRAS, 285, 651 (Paper III)
Winget D. E. et al., 1994, ApJ, 430, 839